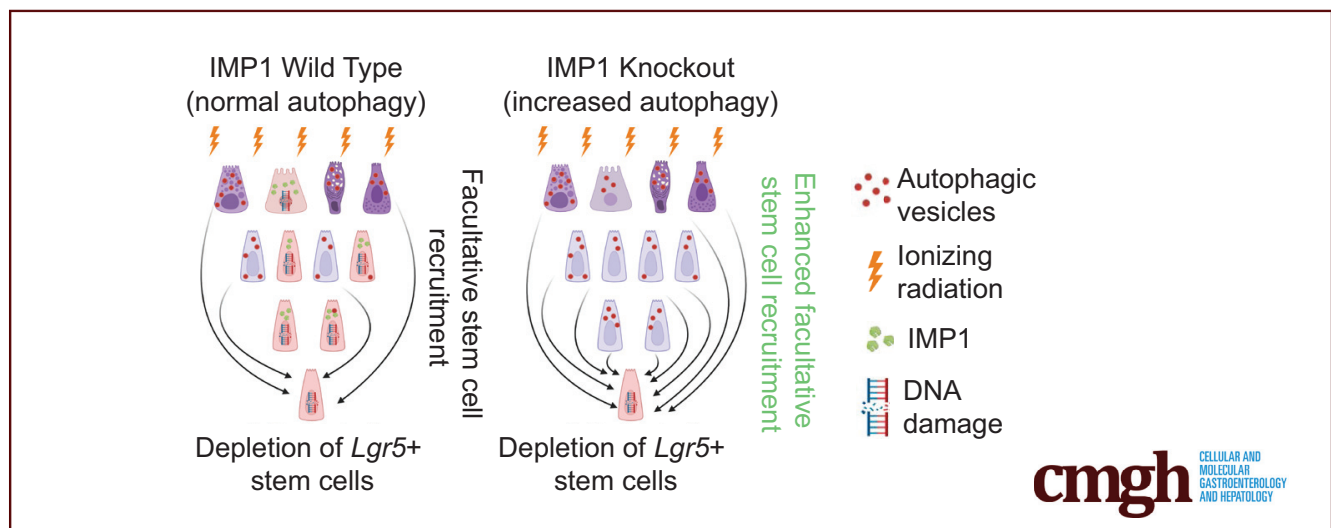


## ORIGINAL RESEARCH

IGF2BP1/IMP1 Deletion Enhances a Facultative Stem Cell State via Regulation of *MAP1LC3B*

Louis R. Parham,<sup>1</sup> Patrick A. Williams,<sup>1</sup> Kay Katada,<sup>1</sup> Shaneice K. Nettleford,<sup>1</sup> Priya Chatterji,<sup>1</sup> Kofi K. Acheampong,<sup>2</sup> Charles H. Danan,<sup>1</sup> Xianghui Ma,<sup>1</sup> Lauren A. Simon,<sup>1</sup> Kaitlyn E. Naughton,<sup>1</sup> Rei Mizuno,<sup>3</sup> Tatiana Karakasheva,<sup>1</sup> Emily A. McMillan,<sup>1</sup> Kelly A. Whelan,<sup>4,5</sup> Donita C. Brady,<sup>6,7</sup> Sydney M. Shaffer,<sup>2,8</sup> and Kathryn E. Hamilton<sup>1</sup>

<sup>1</sup>Division of Gastroenterology, Hepatology, and Nutrition, Department of Pediatrics, Children's Hospital of Philadelphia, University of Pennsylvania Perelman School of Medicine, Philadelphia, Pennsylvania; <sup>2</sup>Department of Pathology and Laboratory Medicine, University of Pennsylvania Perelman School of Medicine, Philadelphia, Pennsylvania; <sup>3</sup>Department of Surgery, Uji-Tokushukai Medical Center, Uji, Kyoto, Japan; <sup>4</sup>Department of Pathology and Laboratory Medicine, Lewis Katz School of Medicine at Temple University, Philadelphia, Pennsylvania; <sup>5</sup>Fels Institute for Cancer Research and Molecular Biology, Lewis Katz School of Medicine at Temple University, Philadelphia, Pennsylvania; <sup>6</sup>Department of Cancer Biology, Perelman School of Medicine, University of Pennsylvania, Philadelphia, Pennsylvania; <sup>7</sup>Abramson Family Cancer Research Institute, Perelman School of Medicine, University of Pennsylvania, Philadelphia, Pennsylvania; and <sup>8</sup>Department of Bioengineering, University of Pennsylvania, Philadelphia, Pennsylvania



## SUMMARY

Intestinal epithelial deletion of the *IGF2* messenger RNA binding protein 1 enhances cell stemness and regeneration in an autophagy-dependent manner. *IGF2* messenger RNA binding protein 1 modulates intestinal autophagy by regulating protein levels of microtubule-associated protein 1 light chain 3 $\beta$ .

**BACKGROUND & AIMS:** The intestinal epithelium interfaces with a diverse milieu of luminal contents while maintaining robust digestive and barrier functions. Facultative intestinal stem cells are cells that survive tissue injury and divide to re-establish the epithelium. Prior studies have shown autophagic state as functional marker of facultative intestinal stem cells, but regulatory mechanisms are not known. The current study evaluated a

post-transcriptional regulation of autophagy as an important factor for facultative stem cell state and tissue regeneration.

**METHODS:** We evaluated stem cell composition, autophagic vesicle content, organoid formation, and in vivo regeneration in mice with intestinal epithelial deletion of the RNA binding protein *IGF2* messenger RNA binding protein 1 (IMP1). The contribution of autophagy to resulting in vitro and in vivo phenotypes was evaluated via genetic inactivation of *Atg7*. Molecular analyses of IMP1 modulation of autophagy at the protein and transcript localization levels were performed using IMP1 mutant studies and single-molecule fluorescent in situ hybridization.

**RESULTS:** Epithelial *Imp1* deletion reduced leucine rich repeat containing G protein coupled receptor 5 cell frequency but enhanced both organoid formation efficiency and in vivo regeneration after irradiation. We confirmed prior studies showing increased autophagy with IMP1 deletion. Deletion of

*Atg7* reversed the enhanced regeneration observed with *Imp1* deletion. IMP1 deletion or mutation of IMP1 phosphorylation sites enhanced expression of essential autophagy protein microtubule-associated protein 1 light chain 3 $\beta$ . Furthermore, immunofluorescence imaging coupled with single-molecule fluorescent in situ hybridization showed IMP1 colocalization with *MAP1LC3B* transcripts at homeostasis. Stress induction led to decreased colocalization.

**CONCLUSIONS:** Depletion of IMP1 enhances autophagy, which promotes intestinal regeneration via expansion of facultative intestinal stem cells. (*Cell Mol Gastroenterol Hepatol* 2024;17:439–451; <https://doi.org/10.1016/j.jcmgh.2023.12.001>)

**Keywords:** Autophagy; regeneration; post-transcriptional gene regulation; intestinal homeostasis.

**L** *gr5*<sup>+</sup> active intestinal stem cells (a-ISCs) are the workhorse cells of the epithelium, ensuring a robust pool of cells to execute digestive and barrier functions in the gut at homeostasis. However, a-ISCs are highly susceptible to cell death owing to DNA damage and inflammation.<sup>1</sup> When a-ISCs are depleted, the intestinal epithelium shows plasticity (functional fluidity in cell identity and state) and can recover via facultative intestinal stem cells (f-ISCs).<sup>2–12</sup> f-ISCs are relatively injury-resistant, and our recent work identified autophagic state (specifically autophagic vesicle levels) as a marker of crypt f-ISCs showing both DNA damage resistance and plasticity.<sup>13</sup> Although cell states that contribute to f-ISC capacity are beginning to be understood, the regulatory factors facilitating these states remain elusive.

RNA-binding proteins (RBPs) can regulate messenger RNA (mRNA) processing, and, ultimately, cell state, by governing interactions of mRNAs with the translation machinery, cytoskeletal network, or other trans-acting factors.<sup>14</sup> RBPs contribute to an essential mechanism for cells to preferentially translate mRNAs in response to external stimuli or stress. Our prior work showed that intestinal epithelial-specific deletion of the RNA binding protein *IGF2* messenger RNA binding protein 1 (IMP1) was associated with increased autophagy in the colon and enhanced colon regeneration after dextran sodium sulfate-mediated epithelial damage.<sup>15</sup> Furthermore, we found *Imp1* deletion was associated with increased regenerative microcolonies after irradiation, and *Imp1* deletion in *Hopx-CreER* expressing f-ISCs recapitulated the same phenotype, highlighting a role for *Imp1* in regulating f-ISC response to irradiation-induced injury.<sup>16</sup> However, the specific role for IMP1 in modulating the balance between a-ISCs and f-ISCs (where IMP1 is primarily expressed), and the mechanistic role for IMP1 in autophagy regulation in the intestine are not known.

In the present study, we evaluated mice with intestinal epithelial *Imp1* deletion to evaluate the frequency of *Lgr5-EGFP* a-ISCs at homeostasis. We used ex vivo organoid formation assays to define the census of single crypt cells with stem cell capacity. We also evaluated the expression of regeneration-associated genes. We then combined deletion


of *Imp1* and the essential autophagy gene *Atg7* to define the requirement of autophagy in *Imp1* deletion-mediated phenotypes in vitro and in vivo using an irradiation injury model. Prior studies defined a direct interaction between IMP1 protein and autophagy transcripts, especially *MAP1LC3B*. We therefore evaluated the molecular mechanisms of IMP1 deletion or IMP1 phosphorylation mutants on microtubule-associated protein 1 light chain 3 $\beta$  (MAP1LC3B) protein expression and mRNA localization at homeostasis and during cell stress. We show that *Imp1* deletion reduces the number of *Lgr5-EGFP* a-ISCs, while at the same time increasing organoid formation efficiency. *Imp1* deletion is associated with an increase in pro-regenerative pathways including autophagy, which we show is required for the regenerative benefit observed with *Imp1* deletion. At the molecular level, IMP1 colocalized with *MAP1LC3B* transcripts at homeostasis, whereas stress reduced this co-localization. Our data support a model in which depletion of IMP1 enhances autophagy, which promotes intestinal regeneration via expansion of facultative intestinal stem cells.

## Results

### Epithelial IMP1 Deletion Reduces a-ISC Frequency While Enhancing Organoid Formation Efficiency

Although we previously reported that *Imp1* deletion in intestinal epithelial cells (IEC, *Imp1*<sup>ΔIEC</sup>) enhances intestinal regeneration after 12 Gy whole-body irradiation,<sup>16</sup> the effects of *Imp1* loss on stem cell dynamics during homeostasis is not known. We therefore evaluated the ability of epithelial cells from *Imp1*-deficient small intestinal crypts to form enteroids when plated as single cells in a 3-dimensional matrix in the presence of stem cell-supporting growth factors. We observed that *Imp1*-deficient crypt epithelial cells can form significantly more organoids than their wild-type counterparts (Figure 1A and B). To determine whether this increased stem cell capacity is a result of an increased

**Abbreviations used in this paper:** a-ISC, active intestinal stem cell; BSA, bovine serum albumin; DAPI, 4',6-diamidino-2-phenylindole; DMEM, Dulbecco's modified Eagle medium; EdU, 5-ethynyl-2'-deoxyuridine; FACS, fluorescence-activated cell sorter; FBS, fetal bovine serum; f-ISC, facultative intestinal stem cell; GFP, green fluorescent protein; HEK, Human Embryonic Kidney; IGF2BP1, IGF2 messenger RNA binding protein 1; IMP1, IGF2 messenger RNA binding protein 1; LC3, microtubule-associated protein light chain 3; Lgr5, leucine rich repeat containing G protein coupled receptor 5; MAP1LC3B, microtubule-associated protein light chain 3beta (gene/transcript); mRNA, messenger RNA; mTORC, mechanistic target of rapamycin complex; NAC, N-acetyl cysteine; PBS, phosphate-buffered saline; pcDNA, plasmid cloning DNA; p-IMP1, IGF2 messenger RNA binding protein 1 phosphorylation; qPCR, quantitative polymerase chain reaction; RBP, RNA-binding protein; smFISH, single-molecule messenger RNA fluorescence in situ hybridization; SSC, side scatter; S181, serine 181; TBS-T, 20.7 mmol/L Tris base; 150.7 NaCl, 0.1% Tween-20, pH 7.6; UEA-1, Ulex Europaeus Agglutinin I; WT, wild-type.

 Most current article

© 2023 The Authors. Published by Elsevier Inc. on behalf of the AGA Institute. This is an open access article under the CC BY-NC-ND license (<http://creativecommons.org/licenses/by-nc-nd/4.0/>).

2352-345X

<https://doi.org/10.1016/j.jcmgh.2023.12.001>

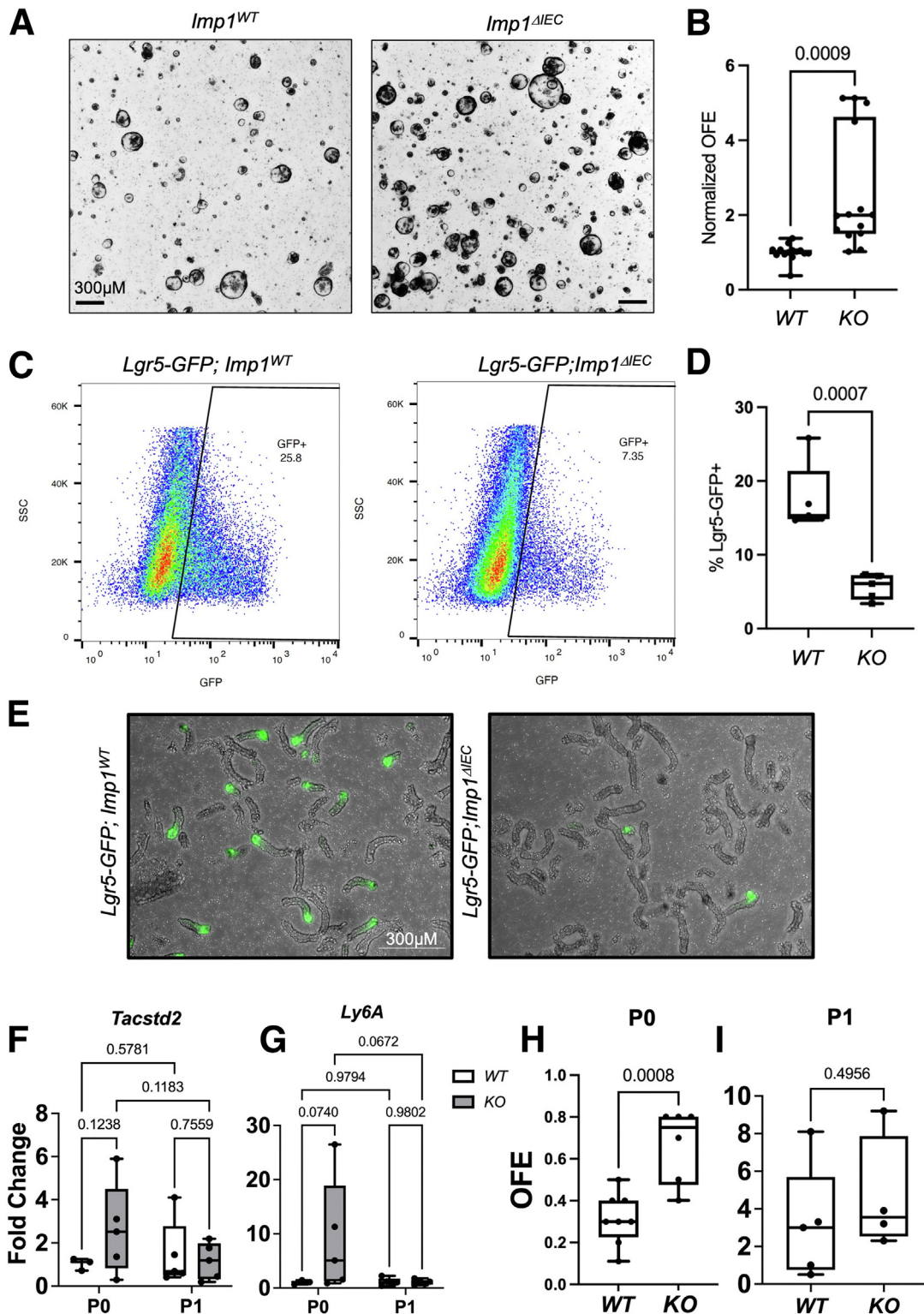


**Figure 1.** *Imp1* deletion enhances organoid formation in intestinal epithelial cells. (A) Brightfield imaging showing that in *Imp1*<sup>ΔIEC</sup> mice, crypt-derived epithelial cells show enhanced organoid formation efficiency (OFE) compared with *Imp1*<sup>WT</sup> mice. (B) Quantification of organoid formation efficiency in *Imp1*<sup>WT</sup> and *Imp1*<sup>ΔIEC</sup> crypt-derived epithelial cells. N = 3 mice/group, 4–6 wells/mouse. P value was generated by a 2-tailed Student *t* test. (C) Plots showing a reduction in Lgr5-GFP+ intestinal stem cells in *Lgr5-GFP; Imp1*<sup>ΔIEC</sup> vs *Lgr5-GFP; Imp1*<sup>WT</sup> mice. (D) Quantification of Lgr5-GFP+ cells in *Lgr5-GFP; Imp1*<sup>ΔIEC</sup> and *Lgr5-GFP; Imp1*<sup>WT</sup> mice. N = 5 mice/group. P value was generated by a 2-tailed Student *t* test. (E) Representative fluorescent imaging of GFP+ crypts in *Lgr5-GFP; Imp1*<sup>ΔIEC</sup> and *Lgr5-GFP; Imp1*<sup>WT</sup> mice. (F and G) qPCR fold change quantification showing *Tacstd2* and *Ly6A* expression in *Imp1*<sup>ΔIEC</sup> vs *Imp1*<sup>WT</sup> organoids during initial plating and subsequent passaging. N = 3–5 mice/group, 4–6 wells/mouse. P value was generated by a 2-way analysis of variance. (H and I) Quantification of organoid formation efficiency in *Imp1*<sup>WT</sup> and *Imp1*<sup>ΔIEC</sup> crypts during initial organoid plating and subsequent passaging. N = 3 mice/group, 4–6 wells/mouse. P value was generated by a 2-tailed Student *t* test. KO, knockout.

frequency of *Lgr5*<sup>+</sup> a-ISCs, we crossed *Imp1*<sup>ΔIEC</sup> mice with *Lgr5-EGFP-IRES-CreERT2* mice and evaluated the percentage of *Lgr5-EGFP* a-ISCs in *Imp1*-deficient crypts cells via flow cytometry. Intriguingly, we observed that *Imp1*<sup>ΔIEC</sup> mice showed a significant reduction of *Lgr5-EGFP*<sup>+</sup> cells compared with their wild-type counterparts (Figure 1C and D). These results were confirmed further with ex vivo imaging showing a significant reduction of *EGFP*<sup>+</sup> crypts in *Imp1*<sup>ΔIEC</sup> mice (Figure 1E).

The establishment of enteroids from single intestinal crypt cells in vitro has been shown previously to recapitulate regenerative aspects of the intestinal epithelium. Upon single-cell plating, cells with stem cell capacity can robustly proliferate to form spherical organoids. Subsequently, symmetry-breaking events occur in these spheres that result in the formation of crypt-like structures that contain the full gamut of intestinal epithelial cell types.<sup>17–20</sup> To determine whether the increased organoid formation efficiency of *Imp1*<sup>ΔIEC</sup> crypt epithelial cells is associated with previously described regenerative response genes, we evaluated the expression of fetal marker genes *Tacstd2* and *Ly6a*, which have been shown to be up-regulated during the in vivo intestinal regenerative response.<sup>21–24</sup> We observed that *Imp1*<sup>ΔIEC</sup> enteroids during initial plating show increased expression of *Tacstd2* and *Ly6a* compared with controls, although these effects were variable and not statistically significant. Moreover, *Tacstd2* and *Ly6a* expression appeared to normalize to wild-type levels during subsequent organoid passaging (Figure 1F and G). In a similar fashion, we observed that the organoid formation efficiency of *Imp1*<sup>ΔIEC</sup> enteroids returned to wild-type levels during subsequent passaging (Figure 1H and I). These results suggest that the enhanced organoid formation capacity of *Imp1*<sup>ΔIEC</sup> crypt epithelial cells is driven by increased expression of genes activated during the intestinal regenerative response, but that this phenotype is not retained in subsequent culture passages.

### *Imp1* Deletion Does Not Affect the Frequency of Secretory Cells During Homeostasis

Injury-resistant f-ISCS are believed to drive regeneration in the intestinal epithelium.<sup>2,4,6,7,9,10,25</sup> Previous literature has shown that f-ISCS are labeled by the expression of *Bmi1*- and *Hopx-CreER*.<sup>2,3,9,25</sup> Our recent study showed that *Hopx-CreER*-marked cells express markers of cells in the secretory lineage.<sup>13</sup> Furthermore, secretory lineages including Paneth cells and enteroendocrine cells have shown f-ISC capacity.<sup>7,10</sup> To determine whether the increased regenerative capacity of *Imp1*<sup>ΔIEC</sup> epithelial cells is the result of increased frequency of *Hopx-CreER*-marked cells, we crossed the *Hopx-CreER;Rosa-LSL-TdTomato* reporter mouse model to *Imp1*<sup>fl/fl</sup> mice (Figure 2A). Our prior work confirmed the feasibility of this model to delete *Imp1*.<sup>16</sup> We observed that *Imp1* deletion did not result in a significant difference in *Hopx-CreER;Rosa-LSL-TdTomato*<sup>+</sup> cells at homeostasis (Figure 2B and C). To explore whether *Imp1* deletion in the intestinal epithelium affects overall secretory cell numbers at homeostasis, we evaluated secretory cell frequency in

*Imp1*<sup>ΔIEC</sup> mice via analysis of cells expressing high levels of CD24 (known to mark Paneth and enteroendocrine cells)<sup>19</sup> as well as Ulex Europaeus Agglutinin I (UEA-1, shown to mark both goblet and Paneth cells).<sup>26</sup> We did not observe a significant difference in the percentage of CD24<sup>high</sup> or UEA-1<sup>+</sup> cells in *Imp1*<sup>ΔIEC</sup> intestinal epithelial cells (Figure 2D–G). Together these data show that *Imp1* loss in the intestinal epithelium does not affect *Hopx-CreER;Rosa-LSL-TdTomato* or secretory cell frequency at homeostasis. As such, we posited that there is an augmented cell state, rather than augmented cell identity, in *Imp1*<sup>ΔIEC</sup> intestinal epithelial cells that fosters f-ISC capacity.

### *Imp1* Deletion Enhances Intestinal Regeneration in an *Atg7*-Dependent Manner

Autophagy flux, or the measurement of degradation activity, can be ascertained by treating cells with lysosomal inhibitors such as chloroquine. An accumulation of the autophagic vesicle marker microtubule-associated protein light chain 3 (LC3)-II or an increase in autophagic vesicles in the presence of lysosomal inhibitors signifies normal degradation activity.<sup>27</sup> We previously showed that *Imp1* deletion in colonic epithelial cells resulted in increased autophagic flux as evidenced by higher LC3-II by immunoblot in *Imp1*<sup>ΔIEC</sup> compared with controls after chloroquine administration. We also previously quantified CytoID<sup>+</sup> (ENZO Life Science) autophagic vesicles in *Imp1*<sup>ΔIEC</sup> intestinal cells using flow cytometry, where we observed an increase in *Imp1*<sup>ΔIEC</sup> compared with wild type.<sup>15</sup> In a separate study, we showed that high autophagic vesicle content is a marker of f-ISCS.<sup>13</sup> Considering this, we reasoned that enhanced stem cell capacity observed in *Imp1*<sup>ΔIEC</sup> mice may be the result of more autophagy in the intestinal epithelium. Staining of *Imp1*<sup>ΔIEC</sup> enteroids with the autophagic vesicle marker CytoID reveals CytoID<sup>+</sup> puncta throughout *Imp1*<sup>ΔIEC</sup> enteroids, whereas wild-type enteroids show more pronounced puncta in crypt regions. Chloroquine treatment resulted in relatively enhanced puncta in both conditions, confirming normal degradation activity in both conditions (Figure 3A and B). These results suggest that *Imp1* deletion may enable a broader number of cells to show autophagic activity at homeostasis and is consistent with a model in which cell state shifts with *Imp1* deletion may underlie enhanced regeneration.

Our next question was whether the increased organoid formation efficiency of *Imp1*-deficient crypt epithelial cells is dependent on autophagy. We generated *Imp1*<sup>ΔIEC</sup> mice with deletion of the essential autophagy gene *Atg7* (*Imp1*<sup>ΔIEC</sup>; *Atg7*<sup>ΔIEC</sup>) (Figure 3E). We observed that *Atg7* deletion abrogates the enhanced organoid formation efficiency observed in *Imp1*<sup>ΔIEC</sup> mice, suggesting that autophagy is required for expanded f-ISC capacity in *Imp1*<sup>ΔIEC</sup> mice (Figure 3C and D). We previously showed that *Imp1* deletion in the intestinal epithelium results in an enhanced regenerative response after 12 Gy whole-body irradiation, as evidenced by an increased level of regenerative microcolonies.<sup>16</sup> Furthermore, we recently showed that intestinal epithelial cells with high levels of autophagic vesicles are

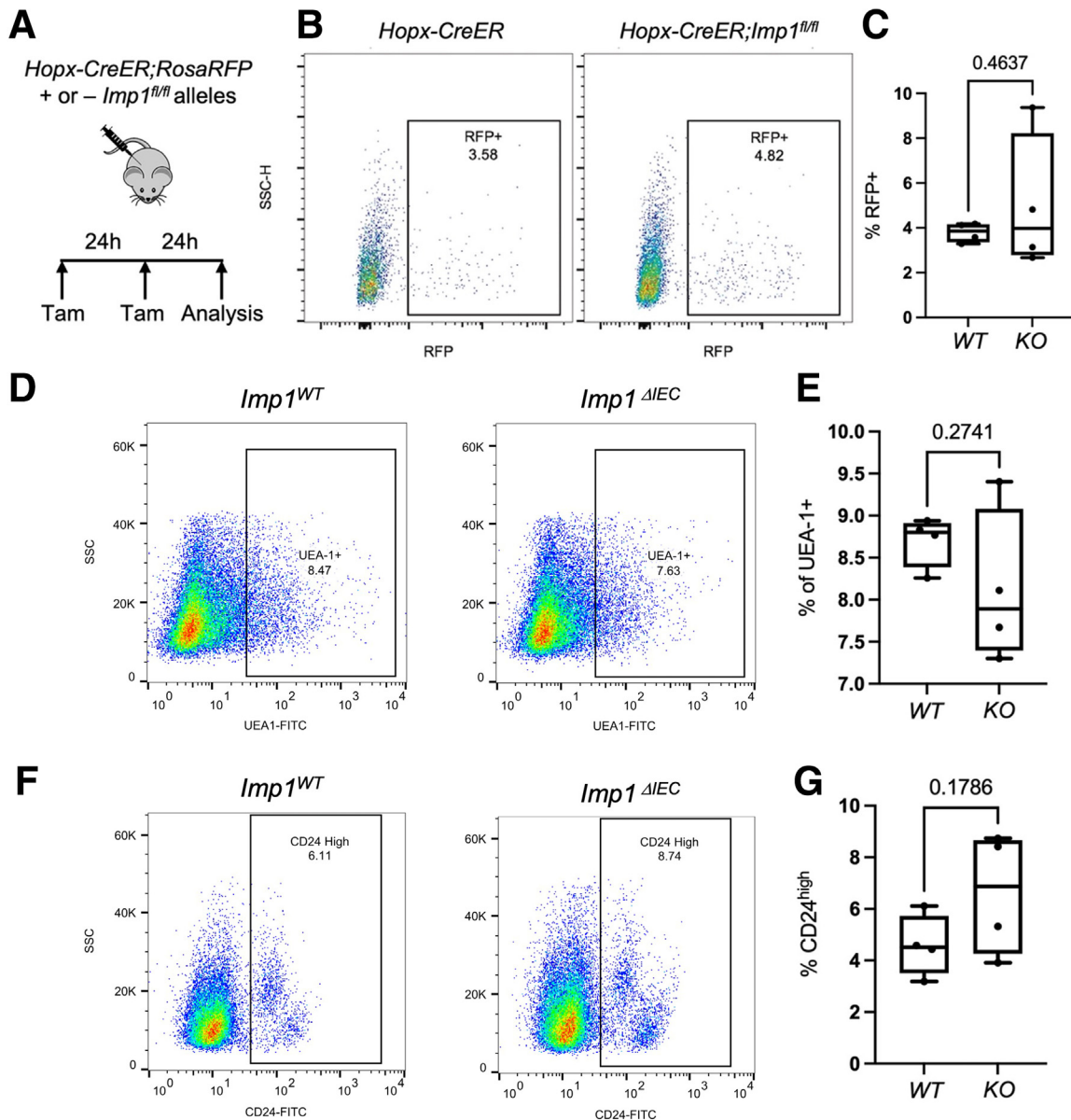


**Figure 2.** *Imp1* loss does not affect secretory cell or f-ISC frequency during homeostasis. (A) Schematic showing tamoxifen treatment scheme for evaluating f-ISC numbers in *Hopx-CreER;Rosa-TdTomato* mice with and without floxed *Imp1* alleles. (B) Representative flow plots showing TdTomato<sup>+</sup> cells in *Hopx-CreER-Rosa-TdTomato* and *Hopx-CreER;Imp1<sup>fl/fl</sup>;Rosa-TdTomato* mice. (C) Quantification of TdTomato<sup>+</sup> cells in *Hopx-CreER-Rosa-TdTomato* and *Hopx-CreER;Imp1<sup>fl/fl</sup>;Rosa-TdTomato* mice. N = 4 mice/group. *P* value was generated by a 2-tailed Student *t* test. (D) Plots showing UEA-1<sup>+</sup> cell numbers in *Imp1<sup>WT</sup>* and *Imp1<sup>ΔIEC</sup>* mice. (E) Quantification of UEA-1<sup>+</sup> cell numbers in *Imp1<sup>WT</sup>* and *Imp1<sup>ΔIEC</sup>*. N = 4 mice/group. *P* value was generated by a 2-tailed Student *t* test. (F) Plots showing CD24 high cell numbers in *Imp1<sup>WT</sup>* and *Imp1<sup>ΔIEC</sup>* mice. (G) Quantification of CD24 high cell numbers in *Imp1<sup>WT</sup>* and *Imp1<sup>ΔIEC</sup>* mice. N = 4 mice/group. *P* value was generated by a 2-tailed Student *t* test. FITC, fluorescein isothiocyanate; RFP, ■■■; Tam, ■■■.

protected against irradiation-induced DNA damage in vivo.<sup>13</sup> To investigate whether enhanced regeneration observed in vivo in *Imp1<sup>ΔIEC</sup>* mice is dependent on autophagy, we evaluated the number of regenerative microcolonies formed 72 hours after 12 Gy ionizing irradiation in *Imp1<sup>ΔIEC</sup>;Atg7<sup>ΔIEC</sup>* mice. We observed that although *Imp1* single deletion results in an increased number of regenerative microcolonies, *Imp1<sup>ΔIEC</sup>;Atg7<sup>ΔIEC</sup>* mice show an abrogated regenerative response, with regenerative microcolony

numbers similar to wild-type animals (Figure 3F and G). Taken together, these results suggest that the enhanced regeneration observed after irradiation in *Imp1<sup>ΔIEC</sup>* mice is dependent on intact autophagy.

### *IMP1 Deletion or Phosphorylation Mutants Increase MAP1LC3B Protein Expression*

We previously showed via ribonucleoprotein immunoprecipitation–quantitative polymerase chain

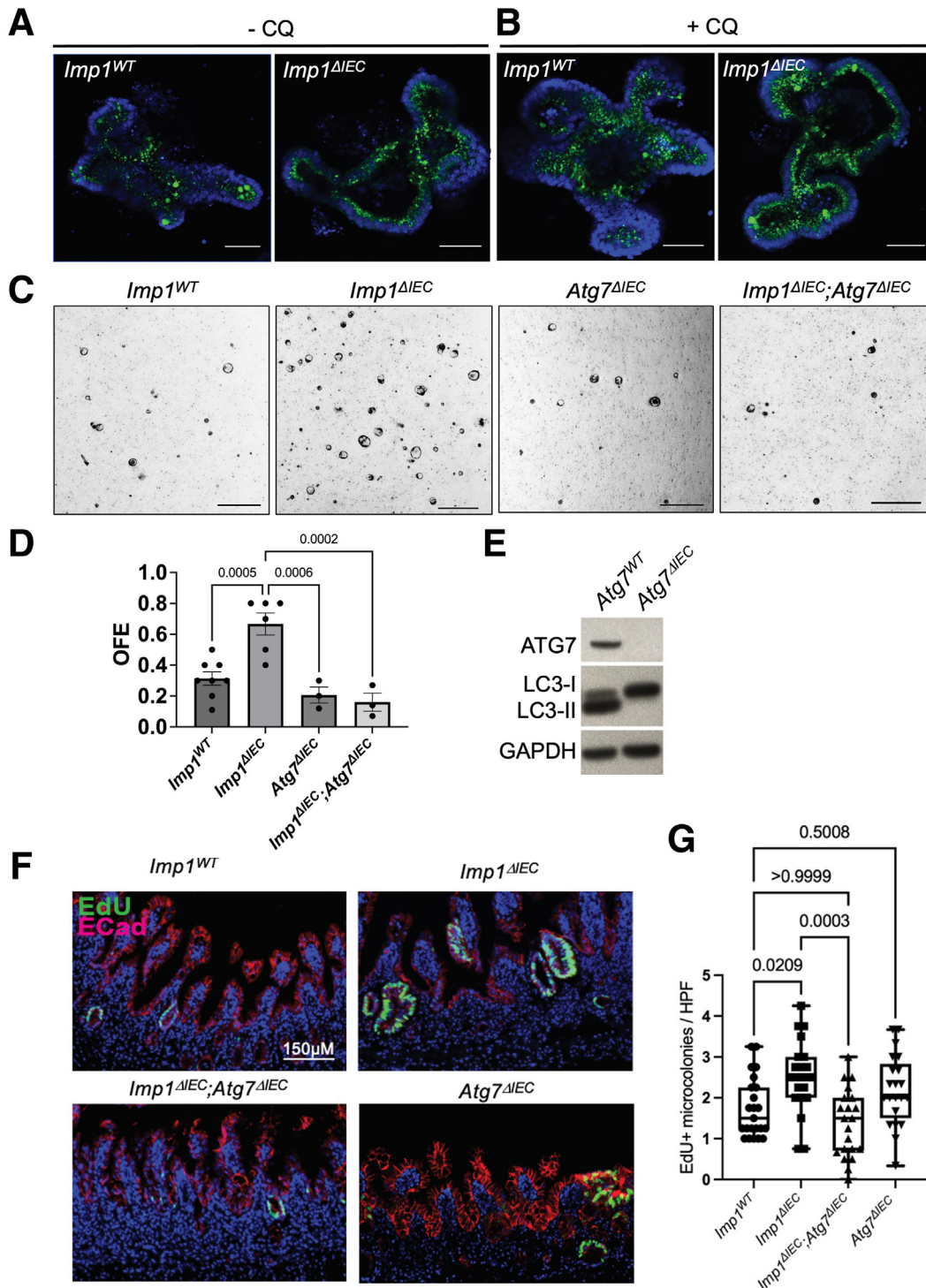


**Figure 3. *Imp1* regulates intestinal regeneration in an autophagy-dependent manner.** (A and B) Representative CytoD staining in *Imp1<sup>ΔIEC</sup>* and *Imp1<sup>WT</sup>* enteroids ± chloroquine (CQ). N = 3 mice/group. (C) Brightfield imaging showing organoid formation efficiency (OFE) in *Imp1<sup>WT</sup>*, *Imp1<sup>ΔIEC</sup>*, *Atg7<sup>ΔIEC</sup>*, and *Imp1<sup>ΔIEC</sup>;Atg7<sup>ΔIEC</sup>* mice. (D) Quantification of organoid formation efficiency in *Imp1<sup>WT</sup>*, *Imp1<sup>ΔIEC</sup>*, *Atg7<sup>ΔIEC</sup>*, and *Imp1<sup>ΔIEC</sup>;Atg7<sup>ΔIEC</sup>* mice. N = 3 mice/group, 4–6 wells/mouse. P value was generated by a 2-tailed Student t test. (E) Western blot from crypts isolated from indicated mice. (F) Representative images of EdU+ foci in indicated mice. (G) Quantification of EdU+ foci per high-powered field in indicated mice. N = 4 mice per genotype, ≥20 high-power fields (HPF) per animal. P values were generated via 1-way analysis of variance with Tukey multiple comparisons. GAPDH, glyceraldehyde-3-phosphate dehydrogenase.

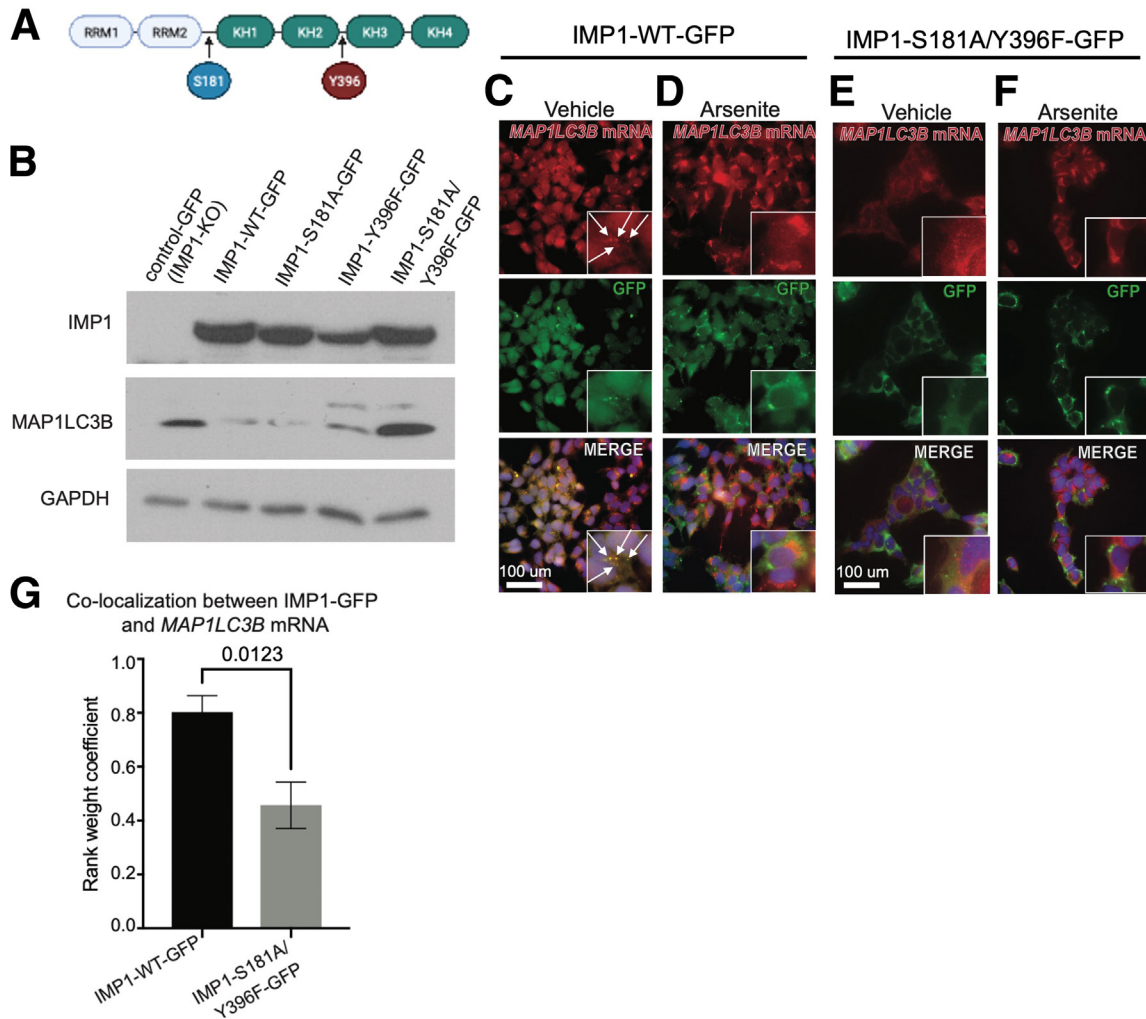


**Figure 4. Imp1 regulates MAP1LC3B in a phosphorylation site-dependent manner.** (A) Schematic showing IMP1 protein structure and phosphorylation sites. (B) Western blot in IMP1-knockout (KO) cells with stable expression of indicated GFP constructs. (C–F) Immunofluorescence and smFISH for IMP1-WT-GFP (green) and MAP1LC3B mRNA (red), respectively, under the indicated conditions. *White arrows* show IMP1-MAP1LC3B co-localization. (G) Rank weight coefficient analysis of MAP1LC3B transcripts and IMP1-GFP colocalization in the indicated cell lines. N = 3 high-power fields across 2 independent experiments. *P* value was generated by a 2-tailed Student *t* test. GAPDH, glyceraldehyde-3-phosphate dehydrogenase.

reaction (qPCR) that IMP1 can bind directly to autophagy transcripts *ATG5*, *ATG3*, and *MAP1LC3B*, and that IMP1 deletion increased MAP1LC3B protein levels.<sup>15</sup> We therefore sought to evaluate molecular mechanisms of IMP1 regulation of MAP1LC3B. IMP1 contains a mechanistic target of rapamycin complex 2 (mTORC2)-dependent phosphorylation site at serine 181 (S181) and a proto-oncogene tyrosine-protein kinase-dependent site at tyrosine 396 (Y396), which can affect translation and/or localization of IMP1 targets (Figure 4A).<sup>28–30</sup> We therefore evaluated the relative contribution of IMP1 phosphorylation (p-IMP1) to its modulation of MAP1LC3B. We generated IMP1-KO Human Embryonic Kidney (HEK) 293 cell lines and introduced the following constructs: *control-GFP* (IMP1-KO) and *IMP1-WT-GFP*, and phosphorylation mutants: *IMP1-S181A-GFP* and *IMP1-Y396F-GFP*, or double-mutant *IMP1-S181A/Y396F-GFP*. We observed increased

MAP1LC3B protein expression in *control-GFP*, *IMP1-Y396F-GFP*, and *IMP1-S181A/Y396F-GFP* mutant cells compared with *IMP1-WT-GFP* or *IMP1-S181A-GFP* (Figure 4B). Taken together, these data suggest that p-IMP1 mutants, and particularly those with *IMP1-Y396F*, recapitulate the effect of IMP1 deletion on MAP1LC3B protein expression.

Because p-IMP1 effects IMP1 localization, which in turn can effect translation of its targets, we used immunofluorescent imaging combined with single-molecule mRNA fluorescence in situ hybridization (smFISH) to evaluate IMP1-MAP1LC3B colocalization. Furthermore, IMP1 can dynamically localize to stress granules in response to various cell stressors, prompting us to use stress granule-inducing sodium arsenite in our analyses.<sup>31</sup> IMP1-wild-type (WT)-green fluorescent protein (GFP) co-localized with *MAP1LC3B* transcripts (Figure 4C, white

arrows) and cell stress induction via arsenite treatment was associated with reduced colocalization of *MAP1LC3B* mRNA and IMP1-WT-GFP (Figure 4D). Colocalization also was reduced in IMP1-S181A/Y396F-GFP cells regardless of stress treatment (Figure 4E and F). The change in colocalization between IMP1 and *MAP1LC3B* was quantified via rank weight coefficient (Figure 4G), showing a significant reduction in colocalization with p-IMP1 mutant compared with WT. Taken together, our data show that IMP1 colocalizes with *MAP1LC3B* transcripts at homeostasis and that derepression occurs in response to the IMP1 phosphorylation state or cell stress.

## Discussion

Over the past 2 decades, the cellular dynamics of the intestinal crypt, including the factors involved in intestinal stem cell maintenance and cellular differentiation, have become very well understood. Canonical Wnt signaling has been shown to be essential for maintaining the intestinal stem cell zone, with genetic disruption of the Wnt signaling pathway in the epithelium resulting in abrogated crypt cell proliferation.<sup>32</sup> Furthermore, it now is appreciated that precise regulation of the Notch signaling pathway is required to maintain a balance of cellular differentiation toward secretory or absorptive cells, with increased Notch signaling resulting in absorptive cell bias, and inhibition resulting in secretory cell differentiation.<sup>33,34</sup> Less is known about the cellular pathways required for f-ISC maintenance and behavior. Recent advances in the field have suggested that activity of mTORC1, an essential regulator of cell growth and metabolism,<sup>35</sup> is an important regulator of f-ISCs in the intestinal epithelium. Yousefi et al<sup>36</sup> showed that mTORC1 activity is correlated inversely with f-ISC survival after 12 Gy ionizing radiation. Furthermore, caloric restriction and fasting (2 cellular states characterized by low metabolic activity and decreased mTORC1 activity) have been shown to result in enhanced intestinal regeneration after irradiation, supporting the premise that mTORC1 activity is an important regulator of f-ISC activity.<sup>36,37</sup> Similarly, high activity of the autophagy pathway (known to be negatively regulated by mTORC1 and induced during calorie restriction) protects intestinal stem cells against irradiation-induced DNA damage.<sup>38</sup> We recently showed that intestinal epithelial cells with high levels of autophagic vesicles show enhanced cellular plasticity and DNA damage resistance.<sup>13</sup> However, mTORC1 activity has been shown to be required for cell-cycle re-entry after tissue damage, suggesting that careful temporal regulation of the mTORC1 and autophagy pathways is required for efficient tissue regeneration. Recently, it was shown that after metaplasia-inducing injury in gastric chief and pancreatic acinar cells, mTORC1 activation is required for cellular proliferation during the regenerative response through a shared program referred to as *palignesis*.<sup>39</sup> The regulatory factors involved in ensuring precise regulation of cell states related to f-ISCs are incompletely understood.

Accumulating literature now has shown that RNA-binding proteins are essential regulators in intestinal

epithelial cells that contribute to intestinal homeostasis, as well as promoting intestinal regeneration after tissue injury.<sup>14</sup> Yousefi et al<sup>40</sup> showed that deletion of the RNA-binding proteins Musashi 1 and 2 is sufficient to completely halt cell cycling in *Hopx-CreER*-labeled f-ISCs, resulting in severely compromised intestinal regeneration after irradiation. Subsequent studies by the same group showed that Musashi RBPs are key regulators of mTORC1.<sup>41</sup> Our group showed that intestinal epithelial-specific deletion of IMP1 results in an enhanced regenerative response after irradiation. Furthermore, *Imp1* deletion in *Hopx-CreER* f-ISCs is sufficient to recapitulate this phenotype, suggesting a stem cell-specific role.<sup>16</sup> We also have shown that *Imp1* deletion in the intestinal epithelium results in increased autophagic activity, pointing toward a potential mechanism by which IMP1 may be regulating intestinal regeneration.<sup>15</sup>

In the present study we evaluated how *Imp1* deletion affects both a-ISCs and f-ISCs during homeostasis, a previously unexplored question, as well as the requirement of autophagy for the enhanced regeneration observed in the absence of *Imp1*. We show that *Imp1* deletion in the intestinal epithelium results in reduced numbers of *Lgr5*+ a-ISCs during homeostasis, as well as increased organoid formation efficiency, in intestinal epithelial cells. Furthermore, we show that combined deletion of *Imp1* and the essential autophagy gene *Atg7* completely abrogates the enhanced organoid formation efficiency observed with *Imp1* single deletion. Furthermore, we show the requirement of intact autophagy for the enhanced regenerative response observed after 12 Gy irradiation in the context of intestinal epithelial-specific *Imp1* loss. Our group has previously shown that high autophagic vesicle content protects against irradiation-induced DNA damage.<sup>13</sup> A potential mechanism by which *Imp1* loss results in enhanced regeneration is through promoting increased f-ISC DNA damage resistance. We intend to explore these hypotheses in subsequent studies.

Prior results from our laboratory have suggested direct binding of IMP1 to multiple autophagy transcripts.<sup>15</sup> In the present article, we evaluated autophagy gene *MAP1LC3B* at the protein level in cells with *IMP1* deletion and found a robust increase. *MAP1LC3B* is a component of the autophagy cascade that, upon conjugation with phosphatidylethanolamine, is essential for autophagosome formation and expansion.<sup>42,43</sup> We also showed that mutation of the IMP1 Y-396 phosphorylation site, either alone or together with mutation in the IMP1 S-181 phosphorylation site, recapitulated the increase in *MAP1LC3B* we observed with *IMP1* deletion. As such, IMP1 appears to regulate the total amount of *MAP1LC3B* protein that is expressed, which could serve as a rheostat for autophagy flux at homeostasis. We used smFISH to evaluate IMP1 protein localization with *MAP1LC3B* transcripts. We found that IMP1 colocalizes with *MAP1LC3B* transcripts at homeostasis, and that both stress induction via sodium arsenite or mutation of p-IMP1 sites is associated with decreased colocalization. Taken together, our results support the notion that IMP1 modulates autophagy at homeostasis via regulation of *MAP1LC3B* translation and localization in a manner dependent, at least in part, on p-IMP1. Sodium arsenite-induced stress decreased



IMP1 localization with *MAP1LC3B* mRNA, suggesting that during stress, IMP1 no longer complexes with *MAP1LC3B* mRNA in the perinuclear region. This is intriguing because recent studies have suggested a functional role for localized translation of specific transcripts in polarized epithelium, such as intestinal epithelial cells.<sup>44</sup> Based on these findings in adherent cells, follow-up studies will evaluate whether IMP1 contributes to specific localization of *MAP1LC3B* mRNA at apical vs basolateral compartments at homeostasis and in response to cell stress.

In summary, in this study we uncovered an IMP1–autophagic state regulatory axis that contributes to regeneration in the intestinal epithelium. More importantly, these findings suggest that IMP1 may be a potential therapeutic target that could be modulated to promote improved intestinal regeneration. Future studies in human tissues or organoids are required to place the IMP1–*MAP1LC3B* regulatory axis into the context of human diseases. Understanding post-transcriptional mechanisms of autophagy regulation in tissues such as the gastrointestinal tract will provide a basis for understanding human disease pathogenesis, and, ultimately, new therapeutic strategies for these diseases.

## Methods

### Animals

All mice used for these studies were between 6 and 12 weeks of age, fed ad libitum, and housed under standard University Laboratory Animal Resources conditions. Both male and female mice were used. The following mice were obtained from Jax Laboratories: *Hopx-CreER* (#017606); *Lgr5-GFP* (#008875); and *R26-tdTomato* (#007909). *Villin-Cre;Imp1<sup>fl/fl</sup>* mice were generated previously and maintained on a C57Bl/6 background. Control mice had floxed, intact alleles (*Imp1<sup>WT</sup>*). *Atg7-floxed* mice were kindly provided by RIKEN BRC through the National Bio-Resource Project of MEXT, Japan. To activate CreERT2-based alleles, mice received 1 mg/kg body weight tamoxifen doses dissolved in corn oil via intraperitoneal injection.

### Isolation of Small Intestinal Crypts and Fluorescence-Activated Cell Sorter Analysis

After the mice were killed, the gastrointestinal tract of the mice was dissected and the most proximal 15 cm of the small intestine was isolated in phosphate-buffered saline (PBS). The tissue was washed briefly in fresh PBS and subsequently was splayed open and transferred to a tube containing 10 mL Hank's balanced salt solution with 1 mmol/L N-acetyl cysteine. After collection, the tissue was vortexed for 15 seconds, followed by a 15-second rest on ice; this was performed repeatedly during a 2-minute period. The tissue then was transferred to a tube containing 10 mL 1X Hank's balanced salt solution with 1 mmol/L NAC and 10 mmol/L EDTA and was placed on a rotator in 4°C for 45 minutes. After the incubation period, the tissue was vortexed for 30 seconds followed by a 30-second rest period on ice; this was performed repeatedly during a 3-minute period. After vortexing, the suspension was

filtered through a 70- $\mu$ m/L strainer and the flow-through was centrifuged at  $300 \times g$  for 3 minutes. To generate a single-cell suspension, the cell pellet was resuspended in a single-cell suspension buffer containing DNase (35  $\mu$ g/mL) and Liberase TH (20  $\mu$ g/mL; Sigma-Aldrich), and was incubated at 37°C for 20 minutes. After digestion, the cells were washed in PBS, resuspended in media containing the desired antibodies, and incubated at 37°C for 30 minutes. The following antibodies and dilutions were used: EpCAM-phosphatidylethanolamine (1:500, cat# 12-5791-82; Thermo Fisher Scientific), CD24-APC (1:500, cat# 101813; BioLegend), and UEA-1 (1:500, cat# FL-1061; Vector Laboratories). Subsequently, the cells were washed in PBS and resuspended in fluorescence-activated cell sorter (FACS) buffer (PBS with 4% fetal bovine serum [FBS]) before FACS analysis. The viability dyes 4',6-diamidino-2-phenylindole (DAPI) and DRAQ7 were used to exclude dead cells. Cells were analyzed and sorted on the FACSJazz and FACSria Fusion sorters. Data analysis was performed using FlowJo, LLC software.

### Small Intestinal Enteroid Culture and Organoid Formation Efficiency

For organoid formation efficiency, intestinal epithelial cells isolated by FACS based on EpCAM positivity (1:500, cat#12-5791-82; Thermo Fisher Scientific) were plated in Matrigel (Corning) droplets at a density of 12,000 cells per 20- $\mu$ L droplet. Matrigel droplets were overlaid with the following medium: advanced Dulbecco's modified Eagle medium (DMEM)/F12 media containing 1X GlutaMAX, 10 mmol/L HEPES buffer, 1X antibiotic–antimycotic, titrated R-spondin 1 and Noggin-containing conditioned media, N-2 supplement, 1x B-27 supplement, 5  $\mu$ mol/L CHIR99021, 1 mmol/L NAC, 50 ng/mL epidermal growth factor, and Y-27632 (10  $\mu$ mol/L). Media was replaced the day after initial plating (day 1), and every other day afterward. All organoid experiments were imaged on day 5 using a Keyence BZ-X all-in-one fluorescence microscope to collect Z-stack images of  $3 \times 3$  focal plane that subsequently was stitched together to form 1 image that encompassed the entire Matrigel droplet. The number of organoids per droplet were counted while making sure to count each structure only once.

### Reverse-Transcription qPCR Analysis in Enteroids

Enteroids were washed with cold DMEM and pelleted. RNA isolations were performed with Quick-RNA MicroPrep kits (R1051; Zymo Research), followed by complementary DNA generation (N8080234, reverse-transcription reagents; Applied Biosystems), and qPCR with TaqMan Fast Universal PCR Master Mix (4444556; Applied Biosystems). The following TaqMan Gene Expression Assays were used: *Ly6a Mm00726565\_s1*, *Tacstd2 Mm00498401\_s1*, and *Gapdh Mm9999915\_g1*. Gene expression was calculated using the  $R = 2^{(-\Delta\Delta Ct)}$  method.

### Live Imaging of Autophagic Vesicles in Enteroids

To evaluate autophagic vesicle accumulation in enteroids, the CytoID Autophagy Detection Kit was used per the manufacturer's protocol, with modifications. Enteroids were passaged 1 day before assays to obtain equivalent plating densities. Three hours before imaging, 2  $\mu\text{g}/\text{mL}$  CytoID and 2  $\mu\text{g}/\text{mL}$  Hoechst33342 (ENZO Life Science) were added to the medium and incubated at 37°C. In chloroquine-treated enteroids, 120  $\mu\text{mol}/\text{L}$  chloroquine (ENZO Life Science) also was added in the medium. After a 3-hour incubation, enteroids were washed with PBS and fresh medium was added. Enteroids were analyzed immediately using confocal microscopy ECLIPSE Ti (Nikon). Six to 10 enteroids per mouse were imaged across 3 mice per genotype. Additional enteroid photos were obtained using a Leica TCS SP8 confocal microscope. Genotype-blinded enteroid imaging of CytoID-positive puncta was performed by RM.

**Generation of HEK293 IMP1-knockout cell lines.** Cells were seeded on a 6-well plate and grown to 60% confluency under standard conditions: growth medium–DMEM with 4.5 g/L glucose and L-glutamine with 10 mmol/L sodium pyruvate (10-017-CV; Corning), 10% FBS (Peak Serum PS-FB1), and penicillin and streptomycin (#15140122; Gibco), in 5% CO<sub>2</sub>. IMP1 deletion was performed using the IGF2BP1 CRISPR/Cas9 knockout plasmid (cat# sc-401703; Santa Cruz) and the IGF2BP1 HDR Plasmid (cat# sc-401703-HDR; Santa Cruz) protocol as described by the manufacturer. Cells were selected using 2  $\mu\text{g}/\text{mL}$  puromycin for 2 passages and knockout was confirmed using Western blot.

**Generation of HEK293-IMP1-GFP mutant cells.** IMP1-S181A-GFP and IMP1-Y396-GFP were generated by site-directed mutagenesis of IMP1-GFP by Genewiz, LLC, and IMP1-S181A/Y396F-GFP was generated by site-directed mutagenesis of IMP1-S181A-GFP by Genewiz, LLC. The HEK293-IMP1-KO cells described previously were used to seed 6-well plates to 60% confluency. Cells then were transfected with plasmid cloning (pc) DNA-GFP, pcDNA-IMP1-GFP, pcDNA-IMP1-S181A-GFP, pcDNA-IMP1-Y396F-GFP, or pcDNA-IMP1-S181A/Y396F-GFP plasmids using Lipofectamine 3000 (Thermo Fisher Scientific) and 2.5  $\mu\text{g}$  DNA/well for 24 hours in DMEM + 10% FBS. After 24 hours' transfection, media was replaced with standard media (DMEM, 10% FBS, penicillin and streptomycin) for 24 hours. Selection with 500  $\mu\text{g}/\text{mL}$  G418 occurred for 4–5 days to enrich for a stably expressing population. After selection, cells were sorted for the highest 5% GFP expression using Zombie Aqua (423101; BioLegend) and the MoFlo Astrios (Beckman Coulter).

**Generation of cell lysates and Western blot.** Cells were lysed with lysis buffer (Cell Lysis Reagent [#9803S; Cell Signaling], Halt Protease Inhibitor Cocktail [#78430; Life Technologies], 1 mmol/L sodium orthovanadate, and 10  $\mu\text{mol}/\text{L}$  sodium fluoride) on ice and spun at 900 relative centrifugal force at 4°C for 10 minutes. Running buffer (final concentration, 62.5 mmol/L; Tris-HCl pH 6.8, 2.5% sodium dodecyl sulfate, 0.002% Bromophenol blue, 5% B-mercaptoethanol, and 10% glycerol) was added to supernatant and boiled for 6 minutes and loaded onto a sodium dodecyl sulfate–polyacrylamide gel electrophoresis with a percentage of 10%, 12.5%, or 15% acrylamide. Samples were run and transferred onto a polyvinylidene difluoride membrane using the Bio-Rad Trans-blot Turbo system and then blocked in either 5% milk or bovine serum albumin (BSA) in 20.7 mmol/L Tris base, 150.7 NaCl, 0.1% Tween-20, pH 7.6 (TBS-T) for 1 hour at room temperature. Primary antibodies were diluted in 5% milk or BSA in TBS-T and incubated with gentle rocking at 4°C for 24 hours. Blots were washed with TBS-T and then incubated in appropriate secondary antibody for 1 hour at room temperature with rocking. After washing, blots were incubated with luminol reagent (sc-2048; Santa Cruz Biotechnology) per the manufacturer's protocol and exposed to autoradiography film. All antibodies are listed in Table 1.

**Immunofluorescence imaging and histology.** Cells were grown on sterilized glass coverslips in 6-well plates under standard conditions until 70% confluent, washed with 1X PBS, and fixed with 4% paraformaldehyde (J19943-K2; Thermo Scientific) for 30 minutes at room temperature. Cells were washed again with PBS and then permeabilized in 0.1% Triton X-100 (Sigma-Aldrich) for 5 minutes and then 0.5% Triton X-100 for 20 minutes before washing with PBS. Cells were blocked in 3% BSA for 1 hour, incubated in primary antibody at 4°C for 24 hours, followed by washing and incubation with secondary antibody for 30 minutes. Cells were stained with DAPI and mounted to coverslips using VECTA-SHIELD Vibrance Antifade Mounting Medium (H-1700-2; Vector Laboratories) and sealed with nail polish (Wet 'n Wild Beauty), and imaged using a Keyence BZ-X700 microscope. Images were processed using a BZ-X Analyzer (Keyence).

Immunofluorescence staining was performed using heat antigen-retrieval in citric acid buffer (pH 6.0) and staining with E-cadherin (610182, 1:1000 dilution; BD Biosciences). 5-ethynyl-2'-deoxyuridine (EdU) staining was performed using the Click-iT EdU Alexa Fluor 488 Imaging Kit (C10337; Thermo Fisher Scientific) as per the manufacturer's protocol. All sections were stained with DAPI

**Table 1.** Antibodies

Antibody	Manufacturer	Catalogue number	Dilution (application, block)
IMP1	Cell Signaling	D33A2	1:1000 (Western blot, milk)
MAP1LC3B (D11)	Cell Signaling	3868	1:1000 (Western blot, milk)
ATGs7	Cell Signaling	D12B11	1:1000 (Western blot, milk)
GAPDH	Santa Cruz	sc-32233	1:2000 (Western blot, milk)
GFP	Novus Bio	NB100-1614	1:200 (immunofluorescence)

GAPDH, glyceraldehyde-3-phosphate dehydrogenase.

**Table 2.** smFISH Probes

agctgcatttttctggttt	MAP1LC3B_1
actgatcgatctcagttggt	MAP1LC3B_2
actactgtttcatgatctgt	MAP1LC3B_3
gctcagttttctgctgaa	MAP1LC3B_4
ccaaagctgaatgtgctcac	MAP1LC3B_5
gtctctctgaaagccttaa	MAP1LC3B_6
acttctaccaaaaaggcgg	MAP1LC3B_7
gatctctctagctgagtaga	MAP1LC3B_8
cttcacaactcaggcctaaa	MAP1LC3B_9
aatgcgttttgcgggggtt	MAP1LC3B_10
cgtttgccaaactgtgatg	MAP1LC3B_11
ttttagtcaggccggtttt	MAP1LC3B_12
taggagtcaggaccttcag	MAP1LC3B_13
tgaggacttgggtgtggtt	MAP1LC3B_14
gaaatgtctaccctgcaag	MAP1LC3B_15
tttctccagggtcttttaag	MAP1LC3B_16
ggcactagttgaaactcaga	MAP1LC3B_17
tgctgctttccgtaacaaca	MAP1LC3B_18
tgactccagagtgcactg	MAP1LC3B_19
tactattttgtttctccc	MAP1LC3B_20
agggagtgtgtcgaatgtt	MAP1LC3B_21
tggatcatccacagcttaa	MAP1LC3B_22
gtgggtaccttttcagtaat	MAP1LC3B_23
ctgtctgacctaaagagtgat	MAP1LC3B_24
tggtgtgggagaattctgat	MAP1LC3B_25
tttccacaactgacatgca	MAP1LC3B_26
gtacggctcttttgctatg	MAP1LC3B_27
ctcttgacattagtatctgt	MAP1LC3B_28
atcacaggtgaaactgagg	MAP1LC3B_29
tactgggaagcactagtctt	MAP1LC3B_30
taaatagtgaaacctatgca	MAP1LC3B_31
cacatagggtctaaagtgtt	MAP1LC3B_32
acaagggtaaagttgtgacct	MAP1LC3B_33
caggtatttcatacacatct	MAP1LC3B_34
ttcccgttacagtaaacag	MAP1LC3B_35
cccagatgcaagaactctgg	MAP1LC3B_36
tgacaggaactcctttaaca	MAP1LC3B_37
tctaaacgagacagtcactg	MAP1LC3B_38
ctgatcacacggtagttaca	MAP1LC3B_39
gaccactcacatgggatata	MAP1LC3B_40
gacagttttaattgtgacct	MAP1LC3B_41

(Invitrogen) and anti-mouse secondary antibodies. No primary negative controls also were used. Scoring of EdU-positive foci, in which a single focus is defined by a cluster of  $\geq 5$  EdU+ cells from a single clone (colony or hyperproliferative crypt), were quantified across at least 20 high-powered fields per animal for a total of 4 mice per genotype. Blinded scoring was performed (P.C. and K.E.H.). **smFISH.** smFISH studies were performed as described previously.<sup>45</sup> Briefly, cells were grown on coverslips in 6-well plates until confluent. For cell stress experiments, cells were treated with 100  $\mu\text{mol/L}$  sodium arsenite for 30

minutes. Cells then were fixed with 4% paraformaldehyde for 10 minutes followed by washing and permeabilization in 70% ethanol overnight at 4°C. Cells were washed in FISH wash buffer (2 $\times$  side scatter, 10% formamide), and then incubated overnight with probes in hybridization buffer (10% dextran sulfate, 10% formamide, 2 $\times$  SSC) at 37°C at a dilution of 1:100. After washing, cells were stained with DAPI followed by washing in 2 $\times$  SSC buffer before being mounted using VECTASHIELD Vibrance Antifade Mounting Medium (H-1700-2; Vector Laboratories). Cells were imaged using an inverted Nikon Ti2-E microscope equipped with a SOLA SE U-nIR light engine (Lumencor), ORCA-Flash 4.0 V3 sCMOS camera (Hamamatsu), with  $\times 60$  Plan-Apo  $\lambda$  (MRD01605) or  $\times 20$  Plan-Apo  $\lambda$  (Nikon MRD00205). Specific probes are listed in Table 2. Images analyses were performed using ImageJ (National Institutes of Health) and CellProfiler.<sup>46,47</sup>

### Statistical Methods

Data were analyzed using unpaired, 2-tailed Student *t* tests, 1-way analysis of variance, or 2-way analysis of variance with post hoc tests (Dunnnett or Tukey), and *P* values are indicated in individual figures. Analyses were performed on data from a minimum of 3 experiments unless otherwise noted, in which case multiple fields were analyzed. All values are presented as means  $\pm$  SEM unless noted otherwise. Specific experimental replicates are described in each figure legend.

### Supplementary Material

Note: To access the supplementary material accompanying this article, go to the full text version at <http://doi.org/10.1016/j.jcmgh.2023.12.001>.

### References

1. Clevers H. The intestinal crypt, a prototype stem cell compartment. *Cell* 2013;154:274–284.
2. Takeda N, Jain R, LeBoeuf MR, et al. Interconversion between intestinal stem cell populations in distinct niches. *Science* 2011;334:1420–1424.
3. Li N, Yousefi M, Nakauka-Ddamba A, et al. Single-cell analysis of proxy reporter allele-marked epithelial cells establishes intestinal stem cell hierarchy. *Stem Cell Rep* 2014;3:876–891.
4. Powell AE, Wang Y, Li Y, et al. The pan-ErbB negative regulator Lrig1 is an intestinal stem cell marker that functions as a tumor suppressor. *Cell* 2012;149:146–158.
5. Gracz AD, Ramalingam S, Magness ST. Sox9 expression marks a subset of CD24-expressing small intestine epithelial stem cells that form organoids in vitro. *Am J Physiol Gastrointest Liver Physiol* 2010;298:G590–G600.
6. Montgomery RK, Carlone DL, Richmond CA, et al. Mouse telomerase reverse transcriptase (mTert) expression marks slowly cycling intestinal stem cells. *Proc Natl Acad Sci U S A* 2011;108:179–184.
7. Yan KS, Gevaert O, Zheng GXY, et al. Intestinal enteroendocrine lineage cells possess homeostatic and

- injury-inducible stem cell activity. *Cell Stem Cell* 2017; 21:78–90.e6.
8. van Es JH, Sato T, van de Wetering M, et al. Dll1+ secretory progenitor cells revert to stem cells upon crypt damage. *Nat Cell Biol* 2012;14:1099–1104.
  9. Sangiorgi E, Capecchi MR. Bmi1 is expressed in vivo in intestinal stem cells. *Nat Genet* 2008;40:915–920.
  10. Yu S, Tong K, Zhao Y, et al. Paneth cell multipotency induced by Notch activation following injury. *Cell Stem Cell* 2018;23:46–59.e5.
  11. Murata K, Jadhav U, Madha S, et al. Ascl2-dependent cell dedifferentiation drives regeneration of ablated intestinal stem cells. *Cell Stem Cell* 2020;26:377–390.e6.
  12. Sheahan BJ, Freeman AN, Keeley TM, et al. Epithelial regeneration after doxorubicin arises primarily from early progeny of active intestinal stem cells. *Cell Mol Gastroenterol Hepatol* 2021;12:119–140.
  13. Johnson NM, Parham LR, Na J, et al. Autophagic state prospectively identifies facultative stem cells in the intestinal epithelium. *EMBO Rep* 2022;23:e55209.
  14. Parham LR, Williams PA, Chatterji P, et al. RNA regulons are essential in intestinal homeostasis. *Am J Physiol Gastrointest Liver Physiol* 2019;316:G197–G204.
  15. Chatterji P, Williams PA, Whelan KA, et al. Post-transcriptional regulation of colonic epithelial repair by RNA binding protein IMP1/IGF2BP1. *EMBO Rep* 2019; 20:e47074.
  16. Chatterji P, Hamilton KE, Liang S, et al. The LIN28B–IMP1 post-transcriptional regulon has opposing effects on oncogenic signaling in the intestine. *Genes Dev* 2018;32:1020–1034.
  17. Lukonin I, Serra D, Challet Meylan L, et al. Phenotypic landscape of intestinal organoid regeneration. *Nature* 2020;586:275–280.
  18. Serra D, Mayr U, Boni A, et al. Self-organization and symmetry breaking in intestinal organoid development. *Nature* 2019;569:66–72.
  19. Sato T, van Es JH, Snippert HJ, et al. Paneth cells constitute the niche for Lgr5 stem cells in intestinal crypts. *Nature* 2011;469:415–418.
  20. Grün D, Lyubimova A, Kester L, et al. Single-cell messenger RNA sequencing reveals rare intestinal cell types. *Nature* 2015;525:251–255.
  21. Mustata RC, Vasile G, Fernandez-Vallone V, et al. Identification of Lgr5-independent spheroid-generating progenitors of the mouse fetal intestinal epithelium. *Cell Rep* 2013;5:421–432.
  22. Yui S, Azzolin L, Maimets M, et al. YAP/TAZ-dependent reprogramming of colonic epithelium links ECM remodeling to tissue regeneration. *Cell Stem Cell* 2018; 22:35–49.e7.
  23. Nusse YM, Savage AK, Marangoni P, et al. Parasitic helminths induce fetal-like reversion in the intestinal stem cell niche. *Nature* 2018;559:109–113.
  24. Wang Y, Chiang I-L, Ohara TE, et al. Long-term culture captures injury-repair cycles of colonic stem cells. *Cell* 2019;179:1144–1159.e15.
  25. Yan KS, Chia LA, Li X, et al. The intestinal stem cell markers Bmi1 and Lgr5 identify two functionally distinct populations. *Proc Natl Acad Sci U S A* 2012;109:466–471.
  26. Parmar N, Burrows K, Vornwald PM, et al. Intestinal-epithelial LSD1 controls goblet cell maturation and effector responses required for gut immunity to bacterial and helminth infection. *PLoS Pathog* 2021;17:e1009476.
  27. Yoshii SR, Mizushima N. Monitoring and measuring autophagy. *Int J Mol Sci* 2017;18:1865.
  28. Dai N, Christiansen J, Nielsen FC, Avruch J. mTOR complex 2 phosphorylates IMP1 cotranslationally to promote IGF2 production and the proliferation of mouse embryonic fibroblasts. *Genes Dev* 2013;27:301–312.
  29. Lambrianidou A, Sereti E, Soupsana K, et al. mTORC2 deploys the mRNA binding protein IGF2BP1 to regulate c-MYC expression and promote cell survival. *Cell Signal* 2021;80:109912.
  30. Hüttelmaier S, Zenklusen D, Lederer M, et al. Spatial regulation of  $\beta$ -actin translation by Src-dependent phosphorylation of ZBP1. *Nature* 2005;438:512–515.
  31. Niewidok B, Igaev M, Pereira da Graca A, et al. Single-molecule imaging reveals dynamic biphasic partition of RNA-binding proteins in stress granules. *J Cell Biol* 2018; 217:1303–1318.
  32. van Es JH, Haegerbarth A, Kujala P, et al. A critical role for the Wnt effector Tcf4 in adult intestinal homeostatic self-renewal. *Mol Cell Biol* 2012;32:1918–1927.
  33. Milano J, McKay J, Dagenais C, et al. Modulation of Notch processing by  $\gamma$ -secretase inhibitors causes intestinal goblet cell metaplasia and induction of genes known to specify gut secretory lineage differentiation. *Toxicol Sci* 2004;82:341–358.
  34. VanDussen KL, Carulli AJ, Keeley TM, et al. Notch signaling modulates proliferation and differentiation of intestinal crypt base columnar stem cells. *Development* 2012;139:488–497.
  35. Saxton RA, Sabatini DM. mTOR signaling in growth, metabolism, and disease. *Cell* 2017;168:960–976.
  36. Yousefi M, Nakauka-Ddamba A, Berry CT, et al. Calorie restriction governs intestinal epithelial regeneration through cell-autonomous regulation of mTORC1 in reserve stem cells. *Stem Cell Rep* 2018;10:703–711.
  37. Richmond CA, Shah MS, Deary LT, et al. Dormant intestinal stem cells are regulated by PTEN and nutritional status. *Cell Rep* 2015;13:2403–2411.
  38. Trentesaux C, Fraudeau M, Pitasi CL, et al. Essential role for autophagy protein ATG7 in the maintenance of intestinal stem cell integrity. *Proc Natl Acad Sci U S A* 2020;117:11136–11146.
  39. Willet SG, Lewis MA, Miao Z-F, et al. Regenerative proliferation of differentiated cells by mTORC1-dependent paligenesis. *EMBO J* 2018;37:e98311.
  40. Yousefi M, Li N, Nakauka-Ddamba A, et al. Msi RNA-binding proteins control reserve intestinal stem cell quiescence. *J Cell Biol* 2016;215:401–413.
  41. Li N, Yousefi M, Nakauka-Ddamba A, et al. The Msi family of RNA-binding proteins function redundantly as intestinal oncoproteins. *Cell Rep* 2015;13:2440–2455.
  42. Ichimura Y, Kirisako T, Takao T, et al. A ubiquitin-like system mediates protein lipidation. *Nature* 2000; 408:488–492.
  43. Nakatogawa H, Ichimura Y, Ohsumi Y. Atg8, a ubiquitin-like protein required for autophagosome formation,

- mediates membrane tethering and hemifusion. *Cell* 2007;130:165–178.
44. Moor AE, Golan M, Massasa EE, et al. Global mRNA polarization regulates translation efficiency in the intestinal epithelium. *Science* 2017;357:1299–1303.
  45. Shaffer SM, Wu M-T, Levesque MJ, Raj A. Turbo FISH: a method for rapid single molecule RNA FISH. *PLoS One* 2013;8:e75120.
  46. McQuin C, Goodman A, Chernyshev V, et al. CellProfiler 3.0: next-generation image processing for biology. *PLoS Biol* 2018;16:e2005970.
  47. Dunn KW, Kamocka MM, McDonald JH. A practical guide to evaluating colocalization in biological microscopy. *Am J Physiol Cell Physiol* 2011;300:C723–C742.

---

Received October 14, 2022. Accepted December 4, 2023.

#### Correspondence

Address correspondence to: Kathryn E. Hamilton, PhD, Children's Hospital of Philadelphia, 903 Abramson Research Building, 3615 Civic Center Boulevard, Philadelphia, Pennsylvania 19104. e-mail: [hamiltonk1@chop.edu](mailto:hamiltonk1@chop.edu).

#### Acknowledgments

The authors thank Drs Joseph Baur and Chris Lengner for helpful discussions and feedback. The authors thank Drs Sarah Andres and Todd Strochlic for providing plasmid backbones used in the present studies.

#### ORCID Authorship Contributions

Louis R. Parham (Conceptualization: Equal; Data curation: Equal; Formal analysis: Equal; Investigation: Lead; Visualization: Equal; Writing – original draft: Equal)

Patrick A. Williams (Conceptualization: Equal; Data curation: Equal; Formal analysis: Equal; Investigation: Lead; Writing – review & editing: Supporting)  
 Kay Katada (Data curation: Supporting; Formal analysis: Supporting)  
 Shaneice K. Nettleford, PhD (Formal analysis: Supporting; Investigation: Supporting; Writing – review & editing: Supporting)  
 Priya Chatterji (Conceptualization: Equal; Data curation: Equal; Formal analysis: Equal; Investigation: Equal)  
 Kofi K. Acheampong (Conceptualization: Supporting; Formal analysis: Supporting)  
 Charles H. Danan (Formal analysis: Supporting; Writing – review & editing: Supporting)  
 Xianghui Ma (Data curation: Supporting; Formal analysis: Supporting)  
 Lauren A. Simon (Data curation: Supporting; Formal analysis: Supporting)  
 Kaitlyn E. Naughton (Data curation: Supporting; Formal analysis: Supporting)  
 Rei Mizuno (Data curation: Supporting; Formal analysis: Supporting)  
 Tatiana A. Karakasheva (Data curation: Supporting; Formal analysis: Supporting)  
 Emily A. McMillan (Data curation: Supporting; Formal analysis: Supporting)  
 Kelly A. Whelan (Formal analysis: Supporting)  
 Donita C. Brady (Formal analysis: Supporting)  
 Sydney M. Shaffer (Data curation: Supporting; Formal analysis: Supporting)  
 Kathryn E. Hamilton, PhD (Conceptualization: Equal; Formal analysis: Equal; Supervision: Lead; Writing – original draft: Equal)

Current address of P.C.: Kojin Therapeutics, Inc, Boston, Massachusetts.

#### Conflicts of interest

The authors disclose no conflicts.

#### Funding

Supported by National Institutes of Health grants R01DK124369 and R21ES031533 (K.E.H.); Institutional Development Funds from Children's Hospital of Philadelphia Research Institute (K.E.H.); and Penn Center for Molecular Studies in Digestive and Liver Diseases National Institutes of Health grants P30DK050306 (K.E.H.), R01DK12115 (K.A.W.), DP5OD028144 (S.M.S.), and F31DK124956 (L.R.P.).